Decoupled Audio-Visual Dataset Distillation

Wenyuan Li Guang Li* Keisuke Maeda Takahiro Ogawa Miki Haseyama

Hokkaido University

Abstract

Audio-Visual Dataset Distillation aims to compress largescale datasets into compact subsets while preserving the performance of the original data. However, conventional Distribution Matching (DM) methods struggle to capture intrinsic cross-modal alignment. Subsequent studies have attempted to introduce cross-modal matching, but two major challenges remain: (i) independently and randomly initialized encoders lead to inconsistent modality mapping spaces, increasing training difficulty; and (ii) direct interactions between modalities tend to damage modalityspecific (private) information, thereby degrading the quality of the distilled data. To address these challenges, we propose DAVDD, a pretraining-based decoupled audio-visual distillation framework. DAVDD leverages a diverse pretrained bank to obtain stable modality features and uses a lightweight decoupler bank to disentangle them into common and private representations. To effectively preserve cross-modal structure, we further introduce Common Intermodal Matching together with a Sample-Distribution Joint Alignment strategy, ensuring that shared representations are aligned both at the sample level and the global distribution level. Meanwhile, private representations are entirely isolated from cross-modal interaction, safeguarding modality-specific cues throughout distillation. Extensive experiments across multiple benchmarks show that DAVDD achieves state-of-the-art results under all IPC settings, demonstrating the effectiveness of decoupled representation learning for high-quality audio-visual dataset distillation. Code will be released.

1. Introduction

Recent advances in deep learning have enabled Deep Neural Networks (DNNs) to deliver substantial performance gains across a wide range of tasks [8]. However, these improvements have been accompanied by a rapid increase in data scale, resulting in prohibitive storage demands and rising

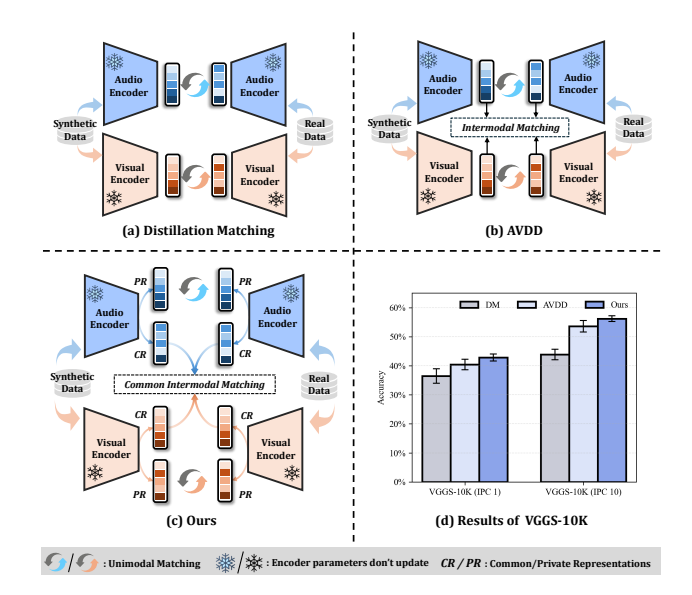


Figure 1. A comparison of architectures for multimodal audiovisual dataset distillation. Subfigures (a), (b), and (c) depict the frameworks of Distillation Matching (DM), Audio-Visual Dataset Distillation (AVDD), and the proposed Decoupled Audio-Visual Dataset Distillation (DAVDD), respectively. Subfigure (d) reports performance on the VGGS-10K dataset under IPC 1 and IPC 10 settings, where DAVDD consistently surpasses prior methods in both accuracy and variance.

computational costs [36]. Dataset Distillation (DD) addresses this issue by synthesizing a compact set of samples that preserves the essential information of the original dataset, thereby reducing data size while maintaining model performance [22, 46]. Over the years, DD research has expanded into multiple branches, including trajectory matching [2, 7, 23, 25], gradient matching [54, 56], distribution matching [29, 53, 55, 57], and generative apporach [12, 26–28, 51], each demonstrating strong potential in applications such as neural architecture search [32, 40], continual learning [13, 39, 50], and privacy-sensitive learning [6, 20, 21, 24].

Among existing approaches, Distribution Matching (DM) has gained particular popularity due to its strong

^{*}Correspondence to: Guang Li (guang@lmd.ist.hokudai.ac.jp)

empirical performance and efficient optimization procedure [55]. DM seeks to align the feature-space distributions of synthetic samples with those of real data, enabling models trained on the distilled dataset to achieve accuracy comparable to training on the full dataset. However, DM has been most successful in single-modal settings such as image classification, where alignment is limited to intra-modal distributions and cross-modal structure is not considered [53].

With the rise of multimodal audio-visual learning [9–11], dataset sizes have expanded even further, yet most existing distillation methods remain confined to single-modality settings. As a result, distillation for audio-visual datasets is still underexplored, and a central challenge persists: how to preserve inter-modal correlations during synthesis. Conventional DM-based methods operate solely through independent within-modality matching, which maintains modality-specific information but entirely overlooks cross-modal relationships (see Fig. 1(a)). To mitigate this limitation, AVDD introduces a cross-modal matching loss that aligns synthetic samples in a joint feature space, enabling the distilled set to retain audio-visual associations better (see Fig. 1(b)) [19].

However, the joint optimization strategy used in AVDD still faces two fundamental limitations. First, it depends on independently initialized encoders with random parameters, causing the visual and audio branches to operate in mismatched embedding spaces. This modality gap significantly complicates cross-modal interaction. Second, enforcing cross-modal matching directly during distillation forces the synthetic samples to satisfy both intra-modal and inter-modal objectives simultaneously, which can introduce conflicting constraints. As a result, modality-private information is often distorted or lost, ultimately reducing the fidelity of the distilled dataset.

To address these limitations, we propose DAVDD, a pretraining-based and fully decoupled audio—visual dataset distillation framework (see Fig. 1(c)). We first pretrain multiple audio and visual encoder pairs, each trained independently, and freeze their weights to construct a diverse pretrained model bank. For every encoder pair, we attach a lightweight decoupler bank composed of two-layer MLPs that project encoder outputs into a shared space. These decouplers disentangle the features into common representations for cross-modal reasoning and private representations, where the original encoder output is preserved to retain modality-specific information.

To enhance shared-feature alignment, we introduce a Sample-Distribution Joint Alignment strategy that combines intra-sample and inter-sample contrastive learning with distribution-level matching. During distillation, we perform intra-modal matching exclusively on private representations, preventing cross-modal interference and safeguarding modality-specific cues. In parallel, we apply Com-

mon Intermodal Matching on the common representations to robustly capture cross-modal correlations within the synthetic dataset. Experiments across multiple benchmarks confirm that DAVDD achieves state-of-the-art performance.

To summarize, our contributions are as follows:

- We propose a novel pretraining-based and decoupled framework for audio-visual dataset distillation that jointly improves efficiency while preserving both modalityprivate information and cross-modal correlations.
- We design a Common Intermodal Matching mechanism that enforces cross-modal alignment while maintaining the integrity of modality-specific private features.
- We introduce a Sample-Distribution Joint Alignment strategy that combines intra-sample and inter-sample contrastive learning with distribution-level matching to substantially enhance the consistency of shared representations.
- We conduct extensive experiments across multiple benchmarks, demonstrating consistent and substantial performance gains over previous state-of-the-art distillation methods.

2. Related Works

2.1. Audio-Visual Learning

Video inherently contains synchronized and complementary audio-visual signals. Leveraging this natural crossmodal consistency, recent work has advanced audio-visual learning across several fronts, including self-supervised representation learning and cross-modal alignment [9–11], sound source separation and localization [4, 33, 59], and event or action recognition with acoustic guidance [52, 60]. These studies collectively show that audio-visual coherence provides both a powerful supervisory signal and a strong inductive bias, enabling the learning of transferable and alignment-aware multimodal representations that consistently outperform unimodal counterparts. In this work, we extend these insights to the dataset distillation setting, aiming to enhance the quality of synthesized audio-visual data for audio-visual event recognition [42].

2.2. Shared-Private Representation Learning

Decomposing multimodal or multi-view data into shared and private representations has proven effective for enhancing downstream performance and is widely adopted across various domains, including multi-view graph learning [31, 34, 35], multimodal sentiment analysis [15, 16, 30, 41], multimodal remote-sensing recognition [14, 37, 47, 48], and related areas [44, 45]. Inspired by this principle, we extend shared–private modeling to multimodal dataset distillation, to capture cross-modal correlations while preserving modality-specific information, thereby avoiding the inherent trade-off between shared and private representations.

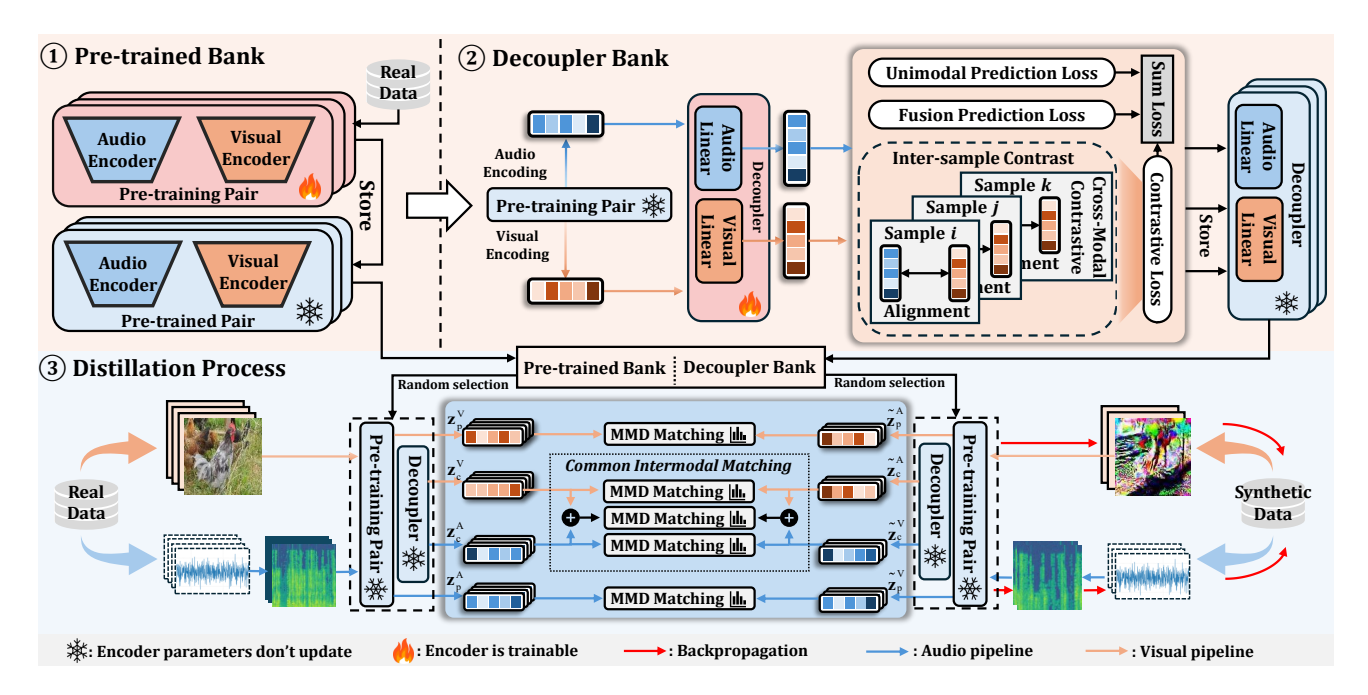


Figure 2. Overview of the DAVDD framework. DAVDD consists of three key components: a pre-trained model bank providing stable and diverse audio-visual encoders, a decoupler bank that projects encoder outputs into shared and private representation spaces, and a decoupled distillation process that performs intra-modal matching on private features and cross-modal alignment on shared features. By combining Sample-Distribution Joint Alignment with Common Intermodal Matching, DAVDD preserves modality-specific information while effectively capturing audio-visual correlations, enabling the synthesis of high-fidelity multimodal datasets.

3. Methodology

3.1. Problem Setting

For the i-th training sample, let \mathbf{a}_i and \mathbf{v}_i denote the audio waveform and the video frame, respectively, and define the paired input as $\mathbf{z}_i = (\mathbf{a}_i, \mathbf{v}_i)$ with label y_i . Given a large audio-visual dataset $\mathcal{D} = \{(\mathbf{z}_i, y_i)\}_{i=1}^{|\mathcal{R}|}$, the objective of audio-visual dataset distillation is to construct a much smaller synthetic set $\widetilde{\mathcal{D}} = \{(\widetilde{\mathbf{z}}_j, \widetilde{y}_j)\}_{j=1}^{|\mathcal{S}|}$, with $|\mathcal{S}| \ll |\mathcal{R}|$, where each synthetic sample $\widetilde{\mathbf{z}}_j = (\widetilde{\mathbf{a}}_j, \widetilde{\mathbf{v}}_j)$ contains both audio and visual components. The distilled set should retain the essential information in \mathcal{D} such that a model trained solely on $\widetilde{\mathcal{D}}$ achieves performance comparable to training on the full dataset. Formally, let ϕ_θ denote a neural network trained on a dataset and $\ell(\cdot,\cdot)$ a loss function such as cross-entropy. Denote by $\theta^*(\mathcal{D})$ and $\theta^*(\widetilde{\mathcal{D}})$ the parameters obtained after training ϕ_θ on \mathcal{D} and $\widetilde{\mathcal{D}}$, respectively. The goal of distillation is to ensure:

$$\mathbb{E}_{(z,y) \sim \mathcal{D}_{\text{test}}} \left[\ell \left(\phi_{\theta^{\star}(\mathcal{D})}(z), y \right) \right] \\ \approx \mathbb{E}_{(z,y) \sim \mathcal{D}_{\text{test}}} \left[\ell \left(\phi_{\theta^{\star}(\widetilde{\mathcal{D}})}(z), y \right) \right]. \tag{1}$$

To operationalize Eq. (1), optimization-driven approaches in dataset distillation typically fall into two camps: (i) metalearning updates that directly refine the synthetic set $\widetilde{\mathcal{D}}$; and (ii) gradient/parameter matching between models trained on

 $\widetilde{\mathcal{D}}$ and on the real data \mathcal{D} . Both are formulated as bi-level programs and thus require differentiating through an inner training loop, which is computationally expensive.

In contrast, DM [55] avoids nested gradients by matching the *representation distributions* induced by random feature extractors on \mathcal{D} and $\widetilde{\mathcal{D}}$. Within this paradigm, alignment can be conducted at the instance level or via moment matching. Instance-wise alignment captures local correspondences but may fail to reflect global corpus-level structure; accordingly, we adopt moment matching, formulated as:

$$\widetilde{\mathcal{D}}^{*} = \arg\min_{\widetilde{\mathcal{D}}} \ \mathbb{E}_{\varphi \sim \mathcal{P}} \left\| \frac{1}{|\mathcal{D}|} \sum_{(\mathbf{z}, y) \in \mathcal{D}} \varphi(\mathbf{z}) - \frac{1}{|\widetilde{\mathcal{D}}|} \sum_{(\widetilde{\mathbf{z}}, \widetilde{y}) \in \widetilde{\mathcal{D}}} \varphi(\widetilde{\mathbf{z}}) \right\|^{2},$$
(2)

where $\varphi \sim \mathcal{P}$ denotes a feature extractor sampled from a distribution (e.g., a randomly initialized deep network without the final linear classification head).

To assess audio-visual dataset distillation [19], we use an audio-visual event recognition proxy. Each sample has audio \mathbf{a} and video \mathbf{v} . An audio encoder ψ^a processes the spectrogram $S(\mathbf{a})$ to obtain an audio feature f^a , while a visual encoder ψ^v maps \mathbf{v} to a visual feature f^v . A fusion operator \mathcal{F} combines them into a joint representation

 $u = \mathcal{F}(f^a, f^v)$, which is then passed to a classifier to produce prediction probabilities **p**. Training follows the standard cross-entropy objective:

$$\mathcal{L}_{CE}(y, \mathbf{p}) = -\sum_{c=1}^{|\mathcal{C}|} y_c \log p_c.$$
 (3)

This proxy assesses whether the synthetic audio-visual data effectively supports multimodal recognition and how different fusion strategies influence performance.

3.2. Overview

In this paper, we propose a pretrained Decoupled Audio–Visual Dataset Distillation (DAVDD) framework. DAVDD performs fine-grained matching in both the common and private representation spaces, enabling the synthesis of a compact audio–visual dataset whose feature distribution closely aligns with that of the original data. An overview of the full architecture is provided in Fig. 2. The key idea is to leverage multiple high-quality pretrained feature extractors and, for each, attach a lightweight decoupler bank that separates encoder outputs into modality-private and cross-modality-common components. This design effectively mitigates the challenges posed by direct crossmodal interaction during matching and supports stable, decoupled optimization across feature spaces.

3.2.1. Pre-trained Bank

We begin by constructing a pre-trained bank composed of multiple audio-visual encoder pairs, each offering a distinct feature perspective for subsequent distillation. This diversity enables multi-view alignment during matching and improves the robustness of the distilled representations. Concretely, we independently train M audio encoders and visual encoders on \mathcal{D} , and store their learned weights as reusable feature extractors. For the m-th pre-trained encoder pair, given an input $(\mathbf{a}_i, \mathbf{v}_i)$, the feature extraction process is defined as:

$$\varphi^m = \left(\psi_m^a(S(\mathbf{a}_i); \, \theta_m^{a\dagger}), \, \psi_m^v(\mathbf{v}_i; \, \theta_m^{v\dagger})\right), \tag{4}$$

where, for $m=1,\ldots,M$, $\theta_m^{a\dagger}$ and $\theta_m^{v\dagger}$ denote the parameters obtained from the independent fits on \mathcal{D} . The pretrained bank can then be represented as:

$$\mathcal{B}_{\text{pre}} = \left\{ \varphi^m \right\}_{m=1}^M. \tag{5}$$

Entries retrieved from $\mathcal{B}_{\mathrm{pre}}$ are kept frozen in downstream stages.

3.2.2. Decoupler Bank

For each $\varphi^m \in \mathcal{B}_{pre}$, a dedicated decoupler bank is attached:

$$\mathcal{B}_{\text{dec}}^{m} = \left\{ \delta^{(m,t)} \right\}_{t=1}^{T}, \\ \delta^{(m,t)} = \left(g_{m,t}^{a}, g_{m,t}^{v} \right),$$
 (6)

where $g_{m,t}^a$ and $g_{m,t}^v$ are lightweight linear maps into a shared space \mathbb{R}^{d_c} . We collect all decoupler banks as:

$$\mathcal{B}_{\text{dec}} = \left\{ \mathcal{B}_{\text{dec}}^m \right\}_{m=1}^M. \tag{7}$$

Given an input $(\mathbf{a}_i, \mathbf{v}_i)$ and the frozen encoders in $\varphi^{(m)}$, the decoupler projections can be represented as:

$$c_{i,m,t}^{a} = g_{m,t}^{a}(\theta_{m}^{a\dagger}),$$

$$c_{i,m,t}^{v} = g_{m,t}^{v}(\theta_{m}^{v\dagger}).$$
(8)

The decouplers are optimized with a joint loss to (i) broaden multi-view coverage across $t=0,\ldots,T$ and (ii) promote a common representation; the objective is deferred to Subsection 3.3.

3.2.3. Distillation Process

Given the original dataset \mathcal{D} and the synthetic dataset for update $\widetilde{\mathcal{D}}$, we first uniformly and randomly sample a pretrained pair φ^m from the $\mathcal{B}_{\mathrm{pre}}$ for each batch of real and synthetic data, and subsequently sample $\delta^{(m,t)}$ from the $\mathcal{B}^m_{\mathrm{dec}}$ to φ^m .

Subsequently, leveraging the sampled φ^m and $\delta^{(m,t)}$, we encode the data. We reinterpret the direct output of φ^m as the private representation, while the output obtained via a secondary encoding through $\delta^{(m,t)}$ is regarded as the modality-common representation, as follows:

$$\mathbf{z}_{p} = \varphi^{m}(\cdot),$$

$$\mathbf{z}_{c} = \delta^{(m,t)}(\mathbf{z}_{p}).$$
(9)

Then, for the *i*-th sample $\mathbf{z}_i = (\mathbf{a}_i, \mathbf{v}_i)$ in the real data, the common representation and private representation can be expressed as:

$$\mathbf{z}_{p}^{A}(i) = \varphi^{m}(S(\mathbf{a}_{i})), \ \mathbf{z}_{c}^{A}(i) = \delta^{(m,t)}(\mathbf{z}_{p}^{A}(i)),$$
$$\mathbf{z}_{p}^{V}(i) = \varphi^{m}(\mathbf{v}_{i}), \ \mathbf{z}_{c}^{V}(i) = \delta^{(m,t)}(\mathbf{z}_{p}^{V}(i)),$$
(10)

where $\mathbf{z}_p^A(i)$ and $\mathbf{z}_c^A(i)$ denote the private and common representations of the audio modality for the *i*-th sample, respectively, and $\mathbf{z}_p^V(i)$ and $\mathbf{z}_c^V(i)$ denote the private and common representations of the visual modality for the *i*-th sample, respectively.

Similarly, for the j-th sample of the synthetic data $\tilde{\mathbf{z}}_j = (\tilde{\mathbf{a}}_j, \tilde{\mathbf{v}}_j)$, the common and private representations can be formulated as follows:

$$\tilde{\mathbf{z}}_{p}^{A}(j) = \varphi^{m}(S(\tilde{\mathbf{a}}_{j})), \, \tilde{\mathbf{z}}_{c}^{A}(j) = \delta^{(m,t)}(\tilde{\mathbf{z}}_{p}^{A}(j)), \\
\tilde{\mathbf{z}}_{p}^{V}(j) = \varphi^{m}(\tilde{\mathbf{v}}_{j}), \, \tilde{\mathbf{z}}_{c}^{V}(j) = \delta^{(m,t)}(\tilde{\mathbf{z}}_{p}^{V}(j)),$$
(11)

where $\tilde{\mathbf{z}}_p^A(j)$ and $\tilde{\mathbf{z}}_c^A(j)$ denote the private and common representations of the audio modality for the j-th synthetic sample, respectively, and $\tilde{\mathbf{z}}_p^V(j)$ and $\tilde{\mathbf{z}}_c^V(j)$ denote the private and common representation of the visual modality for the j-th synthetic sample.

Private Representation Matching For the private representation branch, DAVDD follows the unimodal structure of DM and does not introduce any cross-modal interaction. Instead, it independently matches the audio and visual private representations of the real and synthetic data. This design ensures that modality-specific cues are preserved without being influenced by cross-modal constraints, thereby maintaining the full fidelity of private information encoded in the original dataset. The Private Representation Matching loss \mathcal{L}_{pr} is formulated as:

$$\mathcal{L}_{\text{pr}} = \mathcal{L}_{\text{pr}}^A + \mathcal{L}_{\text{pr}}^V, \tag{12}$$

where \mathcal{L}_{pr}^{A} and \mathcal{L}_{pr}^{V} denote:

$$\mathcal{L}_{pr}^{A} = \left\| \frac{1}{|\mathcal{R}|} \sum_{i=1}^{|\mathcal{R}|} \mathbf{z}_{p}^{A}(i) - \frac{1}{|\mathcal{S}|} \sum_{j=1}^{|\mathcal{S}|} \tilde{\mathbf{z}}_{p}^{A}(j) \right\|^{2}, \tag{13}$$

$$\mathcal{L}_{\text{pr}}^{V} = \left\| \frac{1}{|\mathcal{R}|} \sum_{i=1}^{|\mathcal{R}|} \mathbf{z}_{p}^{V}(i) - \frac{1}{|\mathcal{S}|} \sum_{j=1}^{|\mathcal{S}|} \tilde{\mathbf{z}}_{p}^{V}(j) \right\|^{2}. \tag{14}$$

Moreover, prior studies suggest that shared and private representations may exhibit non-trivial dependencies [1]. By matching private representations independently within each modality, DAVDD preserves these underlying relationships without disrupting modality-specific structure, leading to more robust and faithful synthetic data.

Common Intermodal Matching For the shared-feature branch, we first align the common representations extracted from each unimodal pathway to ensure that both audio and visual modalities in the synthetic data faithfully capture their corresponding cross-modal shared structure. Formally, the common representations are defined as follows:

$$\mathcal{L}_{\text{com}}^{A} = \left\| \frac{1}{|\mathcal{R}|} \sum_{i=1}^{|\mathcal{R}|} \mathbf{z}_{c}^{A}(i) - \frac{1}{|\mathcal{S}|} \sum_{j=1}^{|\mathcal{S}|} \tilde{\mathbf{z}}_{c}^{A}(j) \right\|^{2}, \quad (15)$$

$$\mathcal{L}_{\text{com}}^{V} = \left\| \frac{1}{|\mathcal{R}|} \sum_{i=1}^{|\mathcal{R}|} \mathbf{z}_{c}^{V}(i) - \frac{1}{|\mathcal{S}|} \sum_{j=1}^{|\mathcal{S}|} \tilde{\mathbf{z}}_{c}^{V}(j) \right\|^{2}.$$
 (16)

During the distillation process, the synthetic samples evolve continuously, and the correlation between their audio and visual modalities changes accordingly. To maintain stable cross-modal alignment throughout this optimization, we introduce a modality-shared joint matching objective as an additional consistency constraint. This serves as a secondary mechanism that reinforces the preservation of au-

dio-visual relationships, formulated as follows:

$$\bar{R}_{com}^{AV} = \left[\frac{1}{|\mathcal{R}|} \sum_{i=1}^{|\mathcal{R}|} \mathbf{z}_{c}^{A}(i) + \frac{1}{|\mathcal{R}|} \sum_{i=1}^{|\mathcal{R}|} \mathbf{z}_{c}^{V}(i) \right],$$

$$\bar{S}_{com}^{AV} = \left[\frac{1}{|\mathcal{S}|} \sum_{i=1}^{|\mathcal{S}|} \tilde{\mathbf{z}}_{c}^{A}(j) + \frac{1}{|\mathcal{S}|} \sum_{i=1}^{|\mathcal{S}|} \tilde{\mathbf{z}}_{c}^{V}(j) \right],$$
(17)

$$\mathcal{L}_{com}^{AV} = \|\bar{R}_{com}^{AV} - \bar{S}_{com}^{AV}\|^2.$$
 (18)

Therefore, our Common Intermodal Matching loss \mathcal{L}_{com} is defined as:

$$\mathcal{L}_{com} = \mathcal{L}_{com}^{AV} + \mathcal{L}_{com}^{A} + \mathcal{L}_{com}^{V}. \tag{19}$$

Furthermore, the overall objective of DAVDD combines all components described above. The total distillation loss \mathcal{L} is therefore defined as:

$$\mathcal{L}_{dis} = \lambda_c \mathcal{L}_{com} + \lambda_p \mathcal{L}_{pr}, \tag{20}$$

where λ_c and λ_p are the corresponding weighting factors. The total distillation loss explicitly decouples private and common representation learning, enabling DAVDD to simultaneously preserve modality-specific information and enforce stable cross-modal alignment.

3.3. Decoupling Process

To ensure the spatial or semantic alignment of the shared feature representations between the audio and visual modalities output by the decoupler, while maintaining the semantic validity of these shared components, we design a decoupling process with a joint loss function to impose constraints on them.

Specifically, we first apply a classification loss to the common representations in each modality, guiding the model to learn discriminative shared semantic information. Additionally, a fusion loss is introduced to enhance the synergy and consistency of the shared information across different modalities, thereby ensuring that the semantic information carried by the shared components remains meaningful. The details are as follows:

$$\mathcal{L}_{\text{cls}} = \lambda_{\text{com}} \left(\mathcal{L}_{\text{CE}}(l_a, y) + \mathcal{L}_{\text{CE}}(l_v, y) \right) + \lambda_{\text{fu}} \mathcal{L}_{\text{CE}}(l_{\text{fuse}}, y).$$
(21)

Here, \mathcal{L}_{CE} denotes the Cross-Entropy Loss. The terms l_a , l_v , and l_{fuse} represent the classification logits derived respectively from the audio features, visual features, and the fused features (where the two modalities are concatenated along the feature dimension). Additionally, λ_{com} and λ_{fu} are the weighting parameters corresponding to each component.

Furthermore, we observe that the real dataset exhibits significant intra-class variations and a dispersed shared semantic space, which hinders the semantic representation of the encoded generated dataset [5]. To address this, we introduce inter-sample contrastive learning to construct a unified category-level semantic space. First, define the composite features z_i^{inter} utilized for this loss:

$$z_i^{\text{inter}} = \mathcal{N}(\mathbf{z}_c^A(i) + \mathbf{z}_c^V(i)), \tag{22}$$

where $\mathcal{N}(x) = x/\|x\|_2$, denoting the L2 normalization operation. Therefore, our inter-sample contrastive learning loss is formulated as:

$$\mathcal{L}_{\text{inter}} = \sum_{i \in I} \frac{-1}{|W(i)|}$$

$$\sum_{w \in W(i)} \log \frac{\exp\left(\sin(z_i^{\text{inter}}, z_w^{\text{inter}})/\tau\right)}{\sum_{k \in I \setminus \{i\}} \exp\left(\sin(z_i^{\text{inter}}, z_k^{\text{inter}})/\tau\right)},$$
(23)

where $W(i) = \{w \in I \setminus \{i\} \mid y_w = y_i\}$ denotes the set of positive samples within the batch that share the same class label as sample i (excluding i itself). τ is the temperature hyperparameter.

Sample-Distribution Joint Alignment To achieve more comprehensive alignment between the two modalities and to fully learn the modality correlations, we propose a Sample-Distribution Joint Alignment strategy. This approach not only performs cross-modal alignment at the sample level but also aligns modalities across the overall dataset distribution. Specifically, for sample-level cross-modal alignment, following prior methodologies [38], we treat the alternative modality of the same sample as a positive sample, and the alternative modalities of all other samples within the same batch as negative samples. Given a minibatch of N, the audio-to-visual cross-modal contrastive loss is defined as:

$$\mathcal{L}_{A \to V} = -\frac{1}{N} \sum_{i=1}^{N} \log \frac{\exp(\operatorname{sim} \left(\mathbf{z}_{c}^{A}(i), \mathbf{z}_{c}^{V}(i)\right) / \tau)}{\sum_{j=1}^{N} \exp(\operatorname{sim} \left(\mathbf{z}_{c}^{A}(i), \mathbf{z}_{c}^{V}(j)\right) / \tau)}.$$
(24)

Similarly, the visual-to-audio cross-modal contrastive loss is:

$$\mathcal{L}_{V \to A} = -\frac{1}{N} \sum_{i=1}^{N} \log \frac{\exp(\operatorname{sim} \left(\mathbf{z}_{c}^{V}(i), \mathbf{z}_{c}^{A}(i)\right) / \tau)}{\sum_{j=1}^{N} \exp(\operatorname{sim} \left(\mathbf{z}_{c}^{V}(i), \mathbf{z}_{c}^{A}(j)\right) / \tau)}.$$
(25)

The overall sample-level cross-modal alignment loss is defined as the symmetric average:

$$\mathcal{L}_{\text{intra}} = \frac{1}{2} \left(\mathcal{L}_{A \to V} + \mathcal{L}_{V \to A} \right). \tag{26}$$

Both inter-sample and intra-sample contrastive learning are computed within a mini-batch, and their perspective is therefore constrained by the batch size. To achieve a more global and stable alignment objective, we introduce a distribution-level alignment loss. The core idea of this loss is to align the mean feature of each class in the current batch (μ) with the historically observed cross-modal global class prototypes (P).

For each class c, we maintain exponential moving average (EMA) prototypes for the audio and visual modalities, denoted by P_c^A and P_c^V , respectively. At each training step, we first compute the mean features μ_c^A and μ_c^V for the set of classes $\mathcal{C}_{\mathcal{B}}$ that appear in the current batch \mathcal{B} . The alignment loss is then defined as the cosine distance between the current means and the cross-modal global prototypes, as follows:

$$\mathcal{L}_{\text{align}} = \frac{1}{|\mathcal{C}_{\mathcal{B}}|} \sum_{c \in \mathcal{C}_{\mathcal{B}}} \left[d_{\cos}(\mu_c^A, P_c^V) + d_{\cos}(\mu_c^V, P_c^A) \right]. \tag{27}$$

Here, $d_{\cos}(u,v)=1-u^{\top}v$. P_c^A and P_c^V are treated as fixed targets and are excluded from gradient back-propagation. The EMA prototype bank P is updated asynchronously after the optimizer step (see Appendix A). This mechanism drives the batch-level feature means toward a stable, crossmodal global distribution centroid, thereby substantially enhancing the robustness of the alignment.

Therefore, our overall decoupling loss is:

$$\mathcal{L}_{de} = \mathcal{L}_{cls} + \lambda_{inter} \mathcal{L}_{inter} + \lambda_{intra} \mathcal{L}_{intra} + \lambda_{align} \mathcal{L}_{align}, \quad (28)$$

where λ_{inter} , λ_{intra} , and λ_{align} are the corresponding weighting factors. The decoupling loss provides a unified supervisory signal that enforces discriminative shared semantics, stabilizes cross-modal alignment, and promotes consistent audio-visual structure across both local batches and global feature distributions.

4. Experiments

4.1. Experimental setup

4.1.1. Datasets

We adhere to the dataset processing approach and experimental settings employed by AVDD [19] and accordingly evaluate our method on the three datasets.

VGGS-10K. AVDD [19] curated a subset from VG-GSound [3] named VGGS-10K. This subset randomly samples 10 categories and contains 8,808 training videos and 444 test videos. VGGSound is a large audio-visual dataset comprising approximately 200,000 video clips sourced from YouTube, spanning 309 distinct categories.

MUSIC-21. MUSIC-21 [58] provides synchronized audio-visual recordings of 21 different musical instruments. This study utilizes only the subset corresponding to solo performances. During processing, all video clips were segmented into independent, non-overlapping one-second windows. This subset was randomly partitioned into training, validation, and test sets, containing 146,908, 7,103, and 42,440 samples, respectively.

Method		VGGS-10K			MUSIC-21			AVE	
IPC	1	10	20	1	10	20	1	10	20
Ratio (%)	0.11	0.17	0.83	0.02	0.2	1	0.2	2	10
Random	15.4±1.9	32.0±1.6	45.1±2.3	24.1±4.3	45.8±1.7	54.9±1.9	10.0±1.2	20.0±1.5	26.3±1.0
Herding [49]	$20.8{\pm}2.1$	39.9 ± 1.6	50.2 ± 0.7	26.2 ± 2.0	51.9 ± 1.4	60.0 ± 0.9	11.8 ± 0.4	26.9 ± 0.5	33.0 ± 0.4
DC [56]	18.3±1.4	32.1±0.8	-	22.6±1.1	-	-	10.5±0.4	-	-
DSA [54]	19.3 ± 1.4	36.6 ± 1.0	-	23.0 ± 1.2	-	-	10.8 ± 0.6	-	-
MTT [2]	34.1 ± 3.6	36.8 ± 2.0	51.9 ± 1.3	28.7 ± 1.2	42.3 ± 1.1	-	12.1 ± 0.4	23.2 ± 1.0	-
DM [55]	36.5±2.5	43.9±1.8	49.0±2.4	38.3±1.3	54.8±1.4	61.1±1.3	21.7±1.5	28.1±1.8	32.6±1.0
AVDD [19]	40.2 ± 1.6	54.0 ± 1.8	57.7±1.7	44.2 ± 2.0	66.9 ± 1.2	69.7 ± 0.8	22.7 ± 1.5	35.9 ± 0.9	40.0 ± 1.2

59.1±1.2 45.7±1.8

Table 1. Comparison of different methods on the VGGS-10K, MUSIC-21, and AVE datasets with IPC = 1, 10, and 20.

AVE. The AVE [43] dataset consists of 4,143 video clips distributed across 28 event categories. In the processing pipeline, each clip was segmented into non-overlapping one-second windows, ensuring these windows were temporally aligned with the synchronized annotations. The final data split (train/validation/test) contains 27,726, 3,288, and 3,305 samples, respectively.

41.9+1.2

 56.2 ± 1.0

 68.2 ± 0.8

4.1.2. Implementation Details

DAVDD

Whole Dataset

We follow the processing pipeline used in previous distillation methods [55, 57] and adopt a unified convolutional neural network (ConvNet) [18] architecture for both audio and visual inputs. Specifically, the audio processing branch consists of three basic blocks, each comprising a convolutional layer, a normalization layer, a ReLU activation function, and a pooling layer. For visual inputs with a larger spatial resolution (224 \times 224), the network is extended to five blocks of the same type. During model training, we employ stochastic gradient descent with a momentum of 0.9 for both the pre-training and validation phases, and the learning rate is consistently set to 0.2. The initialization of synthetic data is achieved by selecting audio-visual paired samples using the Herding method [49], and the batch size is fixed at 128 during training. In particular, we incorporate the Factor technique [17, 57] to enhance the representational capacity of the synthetic data, where the factor parameter l is fixed to 2. The raw audio signals are recorded at a sampling rate of 11 kHz and subsequently converted into 128 × 56 log mel-spectrograms, in alignment with the AVDD [19] setup. For more details on the hyperparameter settings, refer to Appendix B.

We compare DAVDD against several representative audio-visual dataset distillation methods, including AVDD [19], DM [55], DC [56], DSA [54], MTT [2], as well as coreset selection methods, Random and Herding [49]. A detailed introduction to all comparison methods is provided in Appendix C. All reported numbers represent the average performance over five independent runs. All our exper-

iments were conducted on a single RTX A6000 Ada GPU.

 37.3 ± 0.6

 52.2 ± 0.4

23.6±1.1

4.2. Main Results

 71.4 ± 0.9

 67.8 ± 0.9

 85.9 ± 0.8

As shown in Table 1, we compare the performance of our method (DAVDD) against several methods on the VGGS-10K [3], MUSIC-21 [58], and AVE [43] datasets. Across all three audiovisual datasets and under varying IPC settings, DAVDD consistently achieves superior performance, significantly outperforming other SOTA methods.

Compared to AVDD, DAVDD demonstrates stable improvements across all datasets. For instance, on VGGS-10K at IPC=1/10/20, DAVDD's performance is higher by 1.7%, 2.2%, and 1.4%, respectively. The corresponding gains on MUSIC-21 are 1.5%, 0.9%, and 1.7%, while on AVE, the improvements range from 0.9% to 1.4% percentage points. The advantage of DAVDD over DM is even more pronounced, particularly on MUSIC-21 at IPC=1, where its performance surpasses DM by over 7%. This result indicates that the proposed method can more effectively distill the semantic correlations within multimodal audiovisual data. Furthermore, as IPC increases from 1 to 20, the performance of all methods exhibits a consistent upward trend. Notably, at high IPC settings, the performance of DAVDD already approaches the level achieved using the full training set, which demonstrates its effectiveness as a robust multimodal dataset distillation approach. Figure 3 shows the visualization of the distilled VGGS-10K dataset. For other distilled datasets, refer to Appendix D.

4.3. Ablation Study

Table 2 presents an effectiveness study conducted on various module combinations of DAVDD, where CIM stands for Common Intermodal Matching. It is important to note that the baseline refers to the original DM framework. Moreover, when the Common Intermodal Matching option is not selected, matching of shared representations occurs only within individual modalities. The experimental results

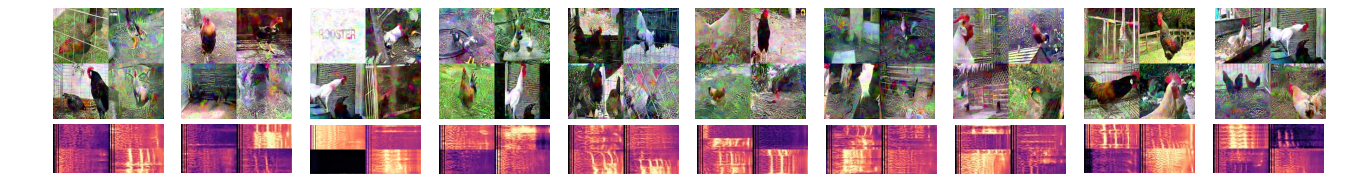


Figure 3. The figure shows the synthesized samples for the class "chicken crowing" from the VGGS-10K dataset with IPC = 10. The top row shows the distilled visual data, while the bottom row shows the corresponding visualized spectrograms of the distilled audio.

demonstrate that the proposed method achieves superior performance. Compared with the original DM approach, randomly sampling pre-trained pairs from the pretrained bank leads to a performance improvement of 5.3%. Furthermore, when the decoupler bank is incorporated, the performance is enhanced by 5.7%, indicating that not only are private representations preserved, but the modality-specific associations between audio and visual modalities are also effectively distilled into the synthesized dataset. To further assess the generalization ability of the distilled data, we additionally conduct cross-architecture evaluations; details are provided in Appendix E.

Table 2. Ablation study results on VGGS-10K with IPC = 10.

	VGGS-10K			
Baseline	Pre-trained Bank	Decoupler Bank	CIM	IPC 10
√	-	-	-	43.9±1.8
✓	✓	=	_	49.2±1.8
✓	✓	✓	_	54.9±1.1
✓	✓	✓	✓	56.2±1.0

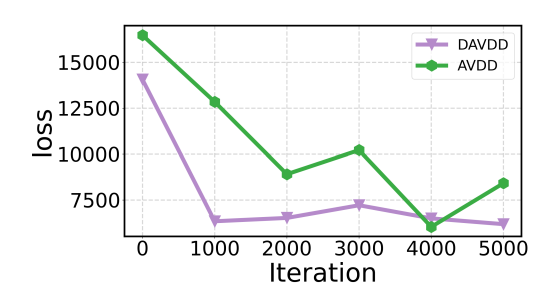


Figure 4. The losses in the AVDD and DAVDD during the distillation process.

4.4. Discussion

As shown in Fig. 4, the loss fluctuations of DAVDD during the distillation process are significantly smaller than those of AVDD, demonstrating the robustness of our method. As shown in Fig. 5, we can observe that when there is no interaction between modalities (i.e., the DM method), the generated images are more similar to the original images, with

only a small number of localized pixel perturbations. This indicates that the modality correlations were not integrated into the synthetic dataset during the distillation process. In contrast, the images distilled using the DAVDD method exhibit greater differences from the original images and contain more perturbations. This ensures that while the images still retain their visual features, the speech-related associations are also distilled effectively. Furthermore, the t-SNE embeddings of our synthetic dataset are provided in Appendix F.

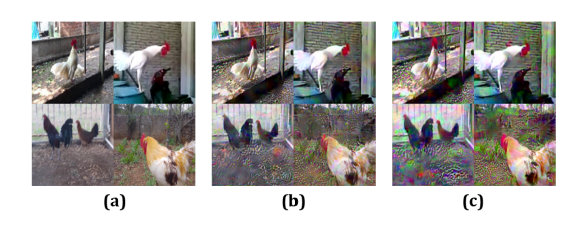


Figure 5. The figure presents the visualization of a sample image from the VGGS-10K dataset at IPC = 10 using different methods. (a) shows the original image, (b) shows the distilled image generated by the DM method, and (c) shows the distilled image generated by our DAVDD method.

5. Conclusion

In this work, we presented DAVDD, a pretraining-based and fully decoupled framework for audio-visual dataset distillation. By combining a diverse pre-trained bank with a lightweight decoupler bank, DAVDD cleanly separates modality-private and cross-modal shared representations, effectively mitigating the instability and interference found in prior audio-visual distillation methods. DAVDD preserves modality-specific information while enforcing stable cross-modal consistency at both sample and distribution levels. This design produces synthetic data with stronger semantic coherence and more reliable modality alignment. Extensive experiments across multiple benchmarks show that DAVDD achieves state-of-the-art performance under all IPC settings, highlighting the effectiveness of decoupled representation learning for scalable, high-quality audio-visual dataset distillation.

References

- [1] Ruichu Cai, Zhifan Jiang, Kaitao Zheng, Zijian Li, Weilin Chen, Xuexin Chen, Yifan Shen, Guangyi Chen, Zhifeng Hao, and Kun Zhang. Learning disentangled representation for multi-modal time-series sensing signals. In ACM Web Conference, pages 3247–3266, 2025. 5
- [2] George Cazenavette, Tongzhou Wang, Antonio Torralba, Alexei A Efros, and Jun-Yan Zhu. Dataset distillation by matching training trajectories. In *IEEE/CVF Conference* on Computer Vision and Pattern Recognition, pages 4750– 4759, 2022. 1, 7
- [3] Honglie Chen, Weidi Xie, Andrea Vedaldi, and Andrew Zisserman. Vggsound: A large-scale audio-visual dataset. In *IEEE International Conference on Acoustics, Speech and Signal Processing*, pages 721–725. IEEE, 2020. 6, 7
- [4] Jiaben Chen, Renrui Zhang, Dongze Lian, Jiaqi Yang, Ziyao Zeng, and Jianbo Shi. iquery: Instruments as queries for audio-visual sound separation. In *IEEE/CVF Conference on Computer Vision and Pattern Recognition*, pages 14675–14686, 2023. 2
- [5] Wenxiao Deng, Wenbin Li, Tianyu Ding, Lei Wang, Hong-guang Zhang, Kuihua Huang, Jing Huo, and Yang Gao. Exploiting inter-sample and inter-feature relations in dataset distillation. In *IEEE/CVF Conference on Computer Vision and Pattern Recognition*, pages 17057–17066, 2024. 6
- [6] Tian Dong, Bo Zhao, and Lingjuan Lyu. Privacy for free: How does dataset condensation help privacy? In *International Conference on Machine Learning*, pages 5378–5396, 2022. 1
- [7] Jiawei Du, Yidi Jiang, Vincent YF Tan, Joey Tianyi Zhou, and Haizhou Li. Minimizing the accumulated trajectory error to improve dataset distillation. In *IEEE/CVF Conference* on Computer Vision and Pattern Recognition, pages 3749– 3758, 2023. 1
- [8] Menghani Gaurav. Efficient deep learning: A survey on making deep learning models smaller, faster, and better. ACM Computing Surveys, 55(12):1–37, 2023. 1
- [9] Mariana-Iuliana Georgescu, Eduardo Fonseca, Radu Tudor Ionescu, Mario Lucic, Cordelia Schmid, and Anurag Arnab. Audiovisual masked autoencoders. In *IEEE/CVF International Conference on Computer Vision*, pages 16144–16154, 2023. 2
- [10] Rohit Girdhar, Alaaeldin El-Nouby, Zhuang Liu, Mannat Singh, Kalyan Vasudev Alwala, Armand Joulin, and Ishan Misra. Imagebind: One embedding space to bind them all. In *IEEE/CVF Conference on Computer Vision and Pattern Recognition*, pages 15180–15190, 2023.
- [11] Yuan Gong, Andrew Rouditchenko, Alexander H. Liu, David Harwath, Leonid Karlinsky, Hilde Kuehne, and James R. Glass. Contrastive audio-visual masked autoencoder. In *International Conference on Learning Representations*, 2023.
- [12] Jianyang Gu, Saeed Vahidian, Vyacheslav Kungurtsev, Haonan Wang, Wei Jiang, Yang You, and Yiran Chen. Efficient dataset distillation via minimax diffusion. In *IEEE/CVF Conference on Computer Vision and Pattern Recognition*, pages 15793–15803, 2024. 1

- [13] Jianyang Gu, Kai Wang, Wei Jiang, and Yang You. Summarizing stream data for memory-constrained online continual learning. In AAAI Conference on Artificial Intelligence, pages 12217–12225, 2024. 1
- [14] Danfeng Hong, Jingliang Hu, Jing Yao, Jocelyn Chanussot, and Xiao Xiang Zhu. Multimodal remote sensing benchmark datasets for land cover classification with a shared and specific feature learning model. *ISPRS Journal of Photogram*metry and Remote Sensing, 178:68–80, 2021. 2
- [15] Nan Jia, Zicong Bai, Tiancheng Xiong, and Mingyang Guo. Multilevel representation disentanglement framework for multimodal sentiment analysis. *IEEE Signal Processing Letters*, 2025. 2
- [16] Ziyu Jia, Fengming Zhao, Yuzhe Guo, Hairong Chen, Tianzi Jiang, and Brainnetome Center. Multi-level disentangling network for cross-subject emotion recognition based on multimodal physiological signals. In *International Joint Conference on Artificial Intelligence*, pages 3069–3077, 2024. 2
- [17] Jang-Hyun Kim, Jinuk Kim, Seong Joon Oh, Sangdoo Yun, Hwanjun Song, Joonhyun Jeong, Jung-Woo Ha, and Hyun Oh Song. Dataset condensation via efficient syntheticdata parameterization. In *International Conference on Machine Learning*, pages 11102–11118. PMLR, 2022. 7
- [18] Alex Krizhevsky, Ilya Sutskever, and Geoffrey E Hinton. Imagenet classification with deep convolutional neural networks. Advances in Neural Information Processing Systems, 25, 2012. 7
- [19] Saksham Singh Kushwaha, Siva Sai Nagender Vasireddy, Kai Wang, and Yapeng Tian. Audio-visual dataset distillation. *Transactions on Machine Learning Research*, 2024. 2, 3, 6, 7
- [20] Guang Li, Ren Togo, Takahiro Ogawa, and Miki Haseyama. Soft-label anonymous gastric x-ray image distillation. In *IEEE International Conference on Image Processing*, pages 305–309, 2020. 1
- [21] Guang Li, Ren Togo, Takahiro Ogawa, and Miki Haseyama. Compressed gastric image generation based on soft-label dataset distillation for medical data sharing. *Computer Meth-ods and Programs in Biomedicine*, 227:107189, 2022. 1
- [22] Guang Li, Bo Zhao, and Tongzhou Wang. Awesome dataset distillation. https://github.com/Guang000/Awesome-Dataset-Distillation, 2022. 1
- [23] Guang Li, Ren Togo, Takahiro Ogawa, and Miki Haseyama. Dataset distillation using parameter pruning. IEICE Transactions on Fundamentals of Electronics, Communications and Computer Sciences, 2023. 1
- [24] Guang Li, Ren Togo, Takahiro Ogawa, and Miki Haseyama. Dataset distillation for medical dataset sharing. In *Proceedings of the AAAI Conference on Artificial Intelligence* (AAAI), Workshop, pages 1–6, 2023. 1
- [25] Guang Li, Ren Togo, Takahiro Ogawa, and Miki Haseyama. Importance-aware adaptive dataset distillation. *Neural Networks*, 2024. 1
- [26] Longzhen Li, Guang Li, Ren Togo, Keisuke Maeda, Takahiro Ogawa, and Miki Haseyama. Generative dataset distillation: Balancing global structure and local details. In *IEEE/CVF Conference on Computer Vision and Pattern Recognition Workshops*, pages 7664–7671, 2024. 1

- [27] Mingzhuo Li, Guang Li, Jiafeng Mao, Takahiro Ogawa, and Miki Haseyama. Diversity-driven generative dataset distillation based on diffusion model with self-adaptive memory. In IEEE International Conference on Image Processing, 2024.
- [28] Mingzhuo Li, Guang Li, Jiafeng Mao, Linfeng Ye, Takahiro Ogawa, and Miki Haseyama. Task-specific generative dataset distillation with difficulty-guided sampling. In IEEE/CVF International Conference on Computer Vision Workshops, 2025. 1
- [29] Wenyuan Li, Guang Li, Keisuke Maeda, Takahiro Ogawa, and Miki Haseyama. Hyperbolic dataset distillation. In *Proceedings of the Advances in Neural Information Processing Systems (NeurIPS)*, 2025. 1
- [30] Zuhe Li, Panbo Liu, Yushan Pan, Weiping Ding, Jun Yu, Haoran Chen, Weihua Liu, Yiming Luo, and Hao Wang. Multimodal sentiment analysis based on disentangled representation learning and cross-modal-context association mining. *Neurocomputing*, 617:128940, 2025. 2
- [31] Junyu Lin, Yan Zheng, Xinyue Chen, Yazhou Ren, Xiaorong Pu, and Jing He. Cross-view contrastive unification guides generative pretraining for molecular property prediction. In ACM International Conference on Multimedia, pages 2108– 2116, 2024. 2
- [32] Dmitry Medvedev and Alexander D'yakonov. Learning to generate synthetic training data using gradient matching and implicit differentiation. In *International Conference on Analysis of Images, Social Networks and Texts*, pages 138– 150, 2021. 1
- [33] Shentong Mo and Yapeng Tian. Audio-visual grouping network for sound localization from mixtures. In *IEEE/CVF Conference on Computer Vision and Pattern Recognition*, pages 10565–10574, 2023. 2
- [34] Yujie Mo, Yajie Lei, Jialie Shen, Xiaoshuang Shi, Heng Tao Shen, and Xiaofeng Zhu. Disentangled multiplex graph representation learning. In *International Conference on Machine Learning*, pages 24983–25005. PMLR, 2023. 2
- [35] Yujie Mo, Zongqian Wu, Yuhuan Chen, Xiaoshuang Shi, Heng Tao Shen, and Xiaofeng Zhu. Multiplex graph representation learning via common and private information mining. In AAAI Conference on Artificial Intelligence, pages 9217–9225, 2023. 2
- [36] Taye Mohammad Mustafa. Understanding of machine learning with deep learning: architectures, workflow, applications and future directions. *Computers*, 12(5):1–27, 2023. 1
- [37] Jiahui Qu, Lijian Zhang, Wenqian Dong, Nan Li, and Yunsong Li. Shared-private decoupling-based multilevel feature alignment semi-supervised learning for hsi and lidar classification. *IEEE Transactions on Geoscience and Remote Sensing*, 2024. 2
- [38] Alec Radford, Jong Wook Kim, Chris Hallacy, Aditya Ramesh, Gabriel Goh, Sandhini Agarwal, Girish Sastry, Amanda Askell, Pamela Mishkin, Jack Clark, et al. Learning transferable visual models from natural language supervision. In *International Conference on Machine Learning*, pages 8748–8763. PmLR, 2021. 6
- [39] Mattia Sangermano, Antonio Carta, Andrea Cossu, and Davide Bacciu. Sample condensation in online continual learn-

- ing. In International Joint Conference on Neural Networks, pages 1–8, 2022. 1
- [40] Felipe Petroski Such, Aditya Rawal, Joel Lehman, Kenneth Stanley, and Jeffrey Clune. Generative teaching networks: Accelerating neural architecture search by learning to generate synthetic training data. In *International Conference on Machine Learning*, pages 9206–9216, 2020. 1
- [41] Haoqin Sun, Shiwan Zhao, Xuechen Wang, Wenjia Zeng, Yong Chen, and Yong Qin. Fine-grained disentangled representation learning for multimodal emotion recognition. In IEEE International Conference on Acoustics, Speech and Signal Processing, pages 11051–11055. IEEE, 2024. 2
- [42] Yapeng Tian, Jing Shi, Bochen Li, Zhiyao Duan, and Chenliang Xu. Audio-visual event localization in unconstrained videos. In *European Conference on Computer Vision*, pages 247–263, 2018.
- [43] Yapeng Tian, Jing Shi, Bochen Li, Zhiyao Duan, and Chenliang Xu. Audio-visual event localization in unconstrained videos. In *European Conference on Computer Vision*, pages 247–263, 2018.
- [44] Beatrice van Amsterdam, Abdolrahim Kadkhodamohammadi, Imanol Luengo, and Danail Stoyanov. Aspnet: Action segmentation with shared-private representation of multiple data sources. In *IEEE/CVF Conference on Computer Vision* and Pattern Recognition, pages 2384–2393, 2023. 2
- [45] Hu Wang, Yuanhong Chen, Congbo Ma, Jodie Avery, Louise Hull, and Gustavo Carneiro. Multi-modal learning with missing modality via shared-specific feature modelling. In *IEEE/CVF conference on computer vision and pattern* recognition, pages 15878–15887, 2023. 2
- [46] Tongzhou Wang, Jun-Yan Zhu, Antonio Torralba, and Alexei A. Efros. Dataset distillation. arXiv preprint arXiv:1811.10959, pages 1–14, 2018. 1
- [47] Yi Wang, Conrad M Albrecht, Nassim Ait Ali Braham, Chenying Liu, Zhitong Xiong, and Xiao Xiang Zhu. Decoupling common and unique representations for multimodal self-supervised learning. In *European Conference on Com*puter Vision, pages 286–303. Springer, 2024. 2
- [48] Tianyu Wei, He Chen, Wenchao Liu, Liang Chen, and Jue Wang. Retain and enhance modality-specific information for multimodal remote sensing image land use/land cover classification. *IEEE Transactions on Geoscience and Remote Sensing*, 2025. 2
- [49] Max Welling. Herding dynamical weights to learn. In International Conference on Machine Learning, pages 1121–1128, 2009.
- [50] Enneng Yang, Li Shen, Zhenyi Wang, Tongliang Liu, and Guibing Guo. An efficient dataset condensation plugin and its application to continual learning. Advances in Neural Information Processing Systems, 36, 2023. 1
- [51] Linfeng Ye, Shayan Mohajer Hamidi, Guang Li, Takahiro Ogawa, Miki Haseyama, and Konstantinos N. Plataniotis. Information-guided diffusion sampling for dataset distillation. In Advances in Neural Information Processing Systems Workshops, 2025. 1
- [52] Heeseung Yun, Ruohan Gao, Ishwarya Ananthabhotla, Anurag Kumar, Jacob Donley, Chao Li, Gunhee Kim,

- Vamsi Krishna Ithapu, and Calvin Murdock. Spherical world-locking for audio-visual localization in egocentric videos. In *European Conference on Computer Vision*, pages 256–274. Springer, 2024. 2
- [53] Hansong Zhang, Shikun Li, Fanzhao Lin, Weiping Wang, Zhenxing Qian, and Shiming Ge. Dance: Dual-view distribution alignment for dataset condensation. arXiv preprint arXiv:2406.01063, 2024. 1, 2
- [54] Bo Zhao and Hakan Bilen. Dataset condensation with differentiable siamese augmentation. In *International Conference on Machine Learning*, pages 12674–12685. PMLR, 2021. 1, 7
- [55] Bo Zhao and Hakan Bilen. Dataset condensation with distribution matching. In *IEEE/CVF Winter Conference on Applications of Computer Vision*, pages 6514–6523, 2023. 1, 2, 3, 7
- [56] Bo Zhao, Konda Reddy Mopuri, and Hakan Bilen. Dataset condensation with gradient matching. arXiv preprint arXiv:2006.05929, 2020. 1, 7
- [57] Ganlong Zhao, Guanbin Li, Yipeng Qin, and Yizhou Yu. Improved distribution matching for dataset condensation. In *IEEE/CVF Conference on Computer Vision and Pattern Recognition*, pages 7856–7865, 2023. 1, 7
- [58] Hang Zhao, Chuang Gan, Wei-Chiu Ma, and Antonio Torralba. The sound of motions. In *IEEE/CVF International Conference on Computer Vision*, pages 1735–1744, 2019. 6, 7
- [59] Jinxing Zhou, Jianyuan Wang, Jiayi Zhang, Weixuan Sun, Jing Zhang, Stan Birchfield, Dan Guo, Lingpeng Kong, Meng Wang, and Yiran Zhong. Audio-visual segmentation. In *European Conference on Computer Vision*, pages 386–403. Springer, 2022. 2
- [60] Jinxing Zhou, Dan Guo, Ruohao Guo, Yuxin Mao, Jingjing Hu, Yiran Zhong, Xiaojun Chang, and Meng Wang. Towards open-vocabulary audio-visual event localization. In IEEE/CVF Conference on Computer Vision and Pattern Recognition, pages 8362–8371, 2025. 2

Decoupled Audio-Visual Dataset Distillation

Supplementary Material

A. Implementation Details of the EMA Prototype Bank Update

To provide a stable and globally consistent cross-modal alignment objective, we maintain a prototype memory bank \mathcal{P} that contains the audio and visual centers of all categories. This memory bank does not participate in gradient back-propagation; instead, it is updated asynchronously after each parameter optimization step. Specifically, for any category c, we first compute the normalized mean feature μ_c within the current mini-batch, and then update the corresponding global prototype P_c using a sample-count-based adaptive momentum strategy:

$$P_c \leftarrow \mathcal{N}(mP_c + (1-m)\mu_c), \tag{29}$$

where $\mathcal{N}(\cdot)$ denotes ℓ_2 normalization. The adaptive momentum coefficient

$$m = \frac{N_{\text{prev}}}{N_{\text{prev}} + N_{\text{curr}}} \tag{30}$$

is dynamically determined by the historical cumulative number of samples $N_{\rm prev}$ and the number of samples $N_{\rm curr}$ of this category in the current mini-batch. This update mechanism essentially computes the cumulative mean over all samples encountered during training, ensuring that the prototypes act as unbiased estimates of the category distribution centroids, thereby providing robust global anchors for the distributional constraints.

B. Other hyperparameter settings

For each dataset, we utilize 40 Pre-trained Pairs, with each pair equipped with four corresponding Decouplers. During the distillation process, all components are aligned within a 6,272-dimensional space. The specific configurations for different loss weights are detailed in Table 3.

Table 3. Loss weights used in our experiments.

Loss weight	Value
λ_c	40
λ_p	80
λ_{com}	2
λ_{fu}	2
λ_{inter}	1
λ_{intra}	3
λ_{align}	1

C. Details of Baseline Methods

Distribution Matching (DM) [55] pioneered the utilization of maximum mean discrepancy to align synthetic data distributions with real data.

Dataset Condensation (DC) [56] addresses this by synthesizing a dataset designed to induce weight gradients that closely mimic those derived from the original large-scale dataset.

Differentiable Siamese Augmentation (DSA) [54] facilitates synthetic data learning by subjecting both real and synthetic data to identical random transformations, while ensuring the augmentations remain differentiable for gradient backpropagation.

Matching Training Trajectories (MTT) [2] matching the training trajectories induced by real and synthetic datasets.

D. Other Distilled Images

We present additional distilled images, as shown in Figures 6 and 7, which correspond to the distilled images for IPC = 1 on the VGGS-10K dataset and for the "driving buses" class with IPC = 10, respectively.



Figure 6. Distilled images on the VGGS-10K dataset with IPC = 1



Figure 7. Distilled images for the "driving buses" class on the VGGS-10K dataset with IPC = 10.

E. Cross-Architecture Experiment

Table 4 reports the cross-architecture generalization performance on the VGGS-10K dataset with IPC = 1. We evaluate the synthetic data distilled by various methods across five distinct architectures: ConvNet, VGG11, LeNet, ResNet18, and AlexNet. As demonstrated in the table, the proposed DAVDD consistently outperforms the baseline methods across the majority of evaluated networks. Specifically, DAVDD achieves state-of-the-art accuracy on

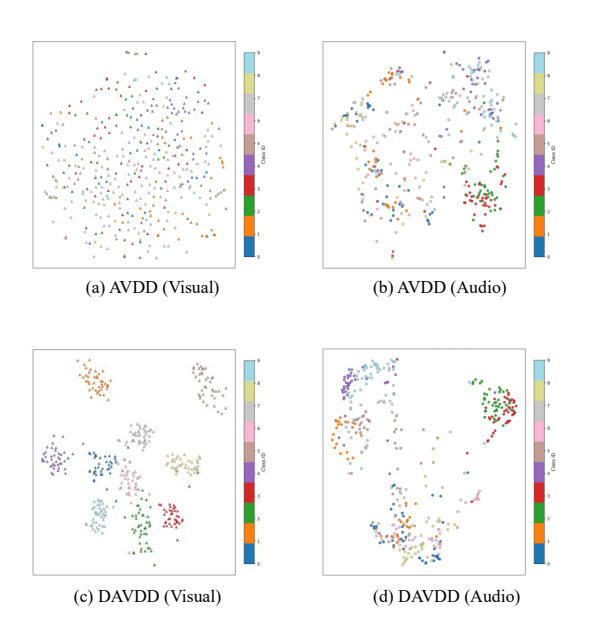


Figure 8. t-SNE visualization of the synthetic AVDD and DAVDD data. (a), (b) show the visual and audio modalities of the AVDD synthetic data, respectively, while (c) and (d) depict the visual and audio modalities of the DAVDD synthetic data.

four out of five architectures, securing top performances of 41.9% on ConvNet and 31.0% on ResNet18. Notably, while AVDD shows competitive performance on LeNet, DAVDD demonstrates significantly stronger generalization capabilities on deeper and more complex architectures, such as VGG11 and ResNet18, surpassing the second-best method by distinct margins.

Table 4. The distillation accuracy of VGGS-10K (IPC = 1) for cross-architecture generalization.

Method	Evaluation Architectures						
	ConvNet	VGG11	LeNet	ResNet18	AlexNet		
MTT	34.1 _{±3.6}	$30.2_{\pm 1.3}$	23.9 _{±3.1}	$24.7_{\pm 1.5}$	$22.6_{\pm 1.4}$		
DM	$36.5_{\pm 2.5}$	$27.0_{\pm 3.6}$	$26.1_{\pm 2.7}$	$22.0_{\pm 1.0}$	$26.7_{\pm 1.8}$		
AVDD	$40.2_{\pm 1.6}$	$34.0_{\pm 1.8}$	$32.4_{\pm 5.2}$	$30.5_{\pm 2.0}$	$31.7_{\pm 2.7}$		
DAVDD	$41.9_{\pm 1.2}$	$34.6 _{\pm 1.6}$	$31.8_{\pm 3.7}$	$31.0_{\pm 1.6}$	$31.9_{\pm 1.9}$		

F. t-SNE visualization

We generate synthetic AVDD and DAVDD data based on VGGS-10K (IPC10), extract features using the same convolutional network as in the main experiments, and visualize their distributions using t-SNE, as shown in Fig. 8. We observe that, in the visual modality, subfigure (c) exhibits more compact clusters and larger inter-class margins, substantially mitigating the class mixing observed in subfigure

(a). This indicates that the DAVDD synthetic data in (c) achieves better visual feature discriminability and class separability than the AVDD synthetic data in (a). In contrast, the difference between subfigures (b) and (d) in the audio modality is less pronounced; nevertheless, the clusters in (d) appear slightly more compact with reduced inter-class overlap, suggesting a modest improvement in audio-wise class separability for DAVDD over AVDD.